RAMAN SPECTROSCOPY AS A TECHNIQUE FOR STUDYING THE STRUCTURE AND MECHANISM OF THE VOLUME PHASE TRANSITION OF POLY(N-ISOPROPYLACRYLAMIDE)

by

Mackenzie L Speer

Bachelors of Science, Gannon University, 2010

Submitted to the Graduate Faculty of the

Dietrich School of Arts and Sciences in partial fulfillment

of the requirements for the degree of

Master of Science

University of Pittsburgh

2013

UNIVERSITY OF PITTSBURGH

DIETRICH SCHOOL OF ARTS AND SCIENCES

This thesis was presented

by

Mackenzie Speer

It was defended on

May 7th, 2013

and approved by

Sean Garrett-Roe, Assistant Professor, Department of Chemistry

Lillian Chong, Associate Professor, Department of Chemistry

Thesis Advisor: Sanford Asher, Distinguished Professor, Department of Chemistry

RAMAN SPECTROSCOPY AS A TECHNIQUE FOR STUDYING THE STRUCTURE AND MECHANISM OF THE VOLUME PHASE TRANSITION OF POLY(N-ISOPROPYLACRYLAMIDE)

Mackenzie Speer, M.S.

University of Pittsburgh, 2013

The volume phase transition, VPT, of poly(N-isopropylacrylamide), PNIPAM, was examined using Raman Spectroscopy. The visible Raman spectra of a solution of PNIPAM microsphere particles were examined at different temperatures above and below the lower critical solution temperature, LCST, of the particles. The frequency shifts of the C-H stretch vibrations of the isopropyl moiety of the NIPAM monomer unit indicated changes in hydration of the PNIPAM. The highest frequency C-H stretch vibrational band derives from the C-H stretch of the methyl groups and downshifts as the solution temperature increases and the polymer collapses indicating dehydration. The C-H stretch of the C-H in the isopropyl moiety shows a downshift at a lower temperature than that of the methyl group, indicating that the disruption of the amide hydration may be the trigger of the cooperative dehydration that the NIPAM monomers experience in the VPT.

Raman spectroscopy was also used to examine the effects of the presence of perchlorate salt on the VPT of PNIAPM and particle aggregation. Using UV Resonance Raman spectroscopy, the hydration of the amide moiety of the NIPAM monomer unit can be closely monitored. The spectra were collected at temperatures above and below the LCST, in the presence and absence of 0.5 M $NaClO_4$. The amide I vibration frequency shift indicated a large increase in the number of amides that are completely dehydrated in the salt solution as compared to the

particles in DI water above the LCST. The salt causes aggregation in the particles as it screens

the repulsion of the charges in the ion-comonomers that normally help to support the

expanded and dispersed particles.

Table of Contents

List of Tables

List of Figures

1.0 Poly(N-isopropylacrylamide) as a Model System for Studying Volume Phase Transitions

Forty five years ago it was first discovered that Poly(N-isopropylacrylamide) (PNIPAM) hydrogels underwent a reversible, discontinuous volume change that was triggered by an increase in temperature[2]. PNIPAM has since become a model system for studying the volume phase transition (VPT) of smart materials that can induce physical or chemical responses to thermal or chemical stimuli [3-7].

These smart-material hydrogels have been further developed and modified to utilize their dramatic change in volume for many different applications. Many have been developed for medical related uses such as controlled drug release[8-10] and artificial muscles[11] while other have been modified for use in chemical sensing[12-16], microfluidic devices[17-19] and to be environmentally responsive[3,20]. Their versatile use stems from their ability to respond to changes in response to many different stimuli including sample temperature[5,7,20-22], pH[8,15], electric field[3], solvent composition[5,6,23,24], or the presence of a specific analyte[13-16].
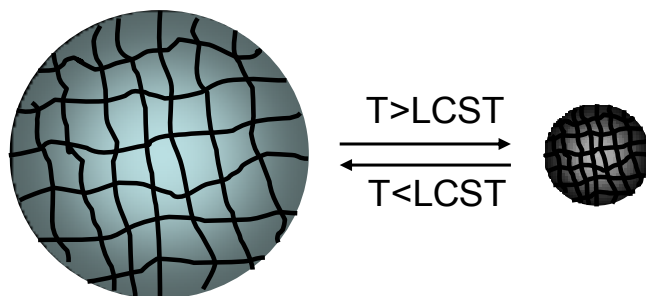
Figure 1. A representation of a cross-linked PNIPAM nanogel particle undergoing a VPT as the temperature changes with respect to the lower critical solution temperature (LCST).

1

The volume phase transition of PNIPAM results from a change in temperature that causes the

nanogel particles to go from a low temperature, swollen state (Fig. 1) that weakly scatters light

below the lower critical solution temperature (LCST) to a collapsed, dehydrated state with

increased turbidity at higher temperatures (Fig. 2). It has been shown that a 3 % cross-linked

nanogel PNIPAM particle is ~300 nm in diameter and swollen in water at 20 °C collapses to a

dehydrated diameter of ~100 nm when the temperature is increased to 35 °C[25]. This 300 nm

particle can expel upward of 10^8 water molecules in as fast as 300 nsec[25-28]. For larger hydrogel

systems, longer times are required for the VPT due to the need for the water to exchange out

of the cross-linked hydrogel system[29]. This VPT has been studied by many different methods on

variations of PNIPAM under different conditions [3-5,22,23,30-39]. The current mechanistic

understanding of the VPT is that it is an entropically-driven, cooperative dehydration of the

amide and hydrophobic groups.

Figure 2. Pictures of the expanded particles at room temperature (left), and the collapsed particles at ~45 °C (right).

The VPT that PNIPAM undergoes is similar to the process of cold denaturation in peptides and proteins. Upon cooling, proteins denature to form a more extended, coil-like conformation and no longer have their non-polar groups buried inside of a collapsed, molten globule conformation. The cold denaturation process occurs when proteins are outside of their narrow range of maximum stability that is typically centered around the host operating temperature[40,41]. When the proteins are in the expanded denatured form, the more polar groups of the protein are solvent exposed. The argument that is made for this globule-to-coil transition of cold denaturation is that it is an entropically-driven process that invokes hydrophobic forces. The argument is further substantiated by the fact that around room temperature, hydrocarbon solubility decreases with temperature increases [42]. This process is difficult to study in proteins, as cold denaturation often occurs below the water freezing point. Therefore, a model system for cold denaturation is needed.

1.1   Previous Work Studying the Volume Phase Transition of PNIPAM

Early studies of PNIPAM and its VPT have been most popularly completed using light scattering[43-45], calorimetry[34,46], dielectric relaxation[38], and viscometry[44]. After the late 1990's, researchers started to utilize IR and Raman spectroscopy as well as theoretical and computational methods to monitor and examine both the polymer and its solvent as the VPT occurs. The aggregation and phase separation of these polymer solutions and microgels has also been studied.

The hydrogen bonding and hydrophobic interactions during the collapse portion of the VPT of PNIPAM have been studied extensively by FTIR. Maeda et al observed that at high temperatures, the vibrational bands assigned to both hydrophobic and hydrophilic sections of the PNIPAM showed characteristic changes that were attributed to the monomers undergoing dehydration [47,48]. The use of attenuated total reflectance infrared spectroscopy (ATR-FTIR) has been used by multiple groups to examine the complex amide I vibration to better understand the hydrogen bonding environment of the amide moieties of the PNIPAM[32]. The authors assign a low-frequency component of the observed amide I vibration band to be amides participating in intramolecular hydrogen bonding between neighboring monomer units. This assignment would indicate that any changes in the intramolecular hydrogen bonding environment during the VPT can be monitored via the low-frequency region of the amide I vibrational band. Ramon et al indicated that changes in the amide I spectral region are due to the breaking of intermolecular hydrogen bonds and the formation of intramolecular hydrogen bonds[49]. The amide I vibration is predominantly from C=O stretching with small amounts of C-N stretch and N-H bend contributing[50] and has shown to be a reliable tool for monitoring the hydrogen bonding environment of the amide moiety[51].

Additional work using vibrational spectroscopy has been done to further study the changes in the PNIPAM as it undergoes a VPT. 2D correlation IR spectroscopy was used to examine the C-H stretch and amide I spectral regions of a PNIPAM hydrogel in D_2O as it is heated and cooled through the VPT[36]. The authors noted that upon cooling the hydrogel back to its original swollen state, the frequency shifts did not return to their original values. This change is thought

4

to be due to the difference in studying an aqueous solution of PNIPAM microgel particles rather than a hydrogel, where the diffusion process of waters re-entering through the swelling polymer network is a limiting factor. Nevertheless, the monitoring of the high-frequency region CH_3 asymmetric stretch showed a clear downshift, while the C=O stretch, amide I, vibrational band showed a clear upshift upon heating of the hydrogel above its LCST. By further examining the amide I vibration, the presence of an intermediate species in the collapse, or heating, process of the VPT was seen, while there was no clear indication of an intermediate in the cooling process. This presence of an isosbestic point indicated that the cooling process is two single states of C=O•••D_2O and C=O•••D-N hydrogen bonding.

Along with the C-H stretch and Amide I regions, many have looked toward the vibrational bands of water to better understand the VPT of PNIPAM as it is well known that the solvent plays a large role in the properties of this transition. Annaka et al have studied the effect of salts on both the low-frequency intermolecular[52] and high-frequency O-H stretch regions[53] of the Raman spectra of aqueous solutions of PNIPAM. Further work on the effect of solvent composition of a PNIPAM solution examined the changes of the low-frequency Raman spectral region as the molar fraction of alcohols and phenols was changed[54]. All three studies determined that the disruption of the hydrogen bonding network around the hydrophobic isopropyl moieties as well as the disruption of the tetrahedral water structure lead to the collapse of PNIPAM. The addition of the salts alters the chemical potential of the solution, which determines the hydration of the PNIPAM. The O-H stretch spectral region of the

interstitial water of the PNIPAM particles was also examined by Raman spectroscopy and shown to have different spectral characteristics than that of the bulk, inter-particle water[55].

Advancements in molecular modeling simulations have led to a greater understanding of the molecular picture of PNIPAM and solvating water molecules around the LCST. Simulations done by Deshmukh et al[56-58] indicate changes in proximal water and the likelihood of different types of hydrogen bonding occurring within the system. The results clearly show, through the use of radial distributions functions, that the carbonyl oxygens of neighboring monomer PNIPAM units increases above the LCST, where the probability of a smaller distance from a carbonyl oxygen of PNIPAM and an oxygen water decreases[56]. This change in distance over the VPT between PNIPAM monomer and water is large when examining the calculated distances from the CH_2 of the PNIPAM backbone to water oxygen[57]. Inter- and intramolecular hydrogen bonding was also examined, finding that the intramolecular C=O•••H-N hydrogen bond is stronger above the LCST and when comparing the two types of polymer-water intermolecular hydrogen bonding, the C=O•••H-O-H is less stable at and above the LCST. Vibrational spectra were also calculated for the proximal to 5th hydration shells and bulk water for both the low-frequency intermolecular and O-H stretch regions showing distinct changes in band shape and position for the various shells.

There is not one specific mechanism for the VPT process of PNIPAM. The general understanding is that there is an entropically-driven process that involves changes in the

hydrogen bonding of the amide groups and solvation of the hydrophobic isopropyl groups of the PNIPAM monomer units.

2.0   Raman Spectroscopy

Vibrational spectroscopy has long been used as a technique for understanding the molecular structures and properties of compounds. Both Raman and IR spectroscopy can yield vital vibrational information about molecules, but there is a clear difference between the two methods. Where in IR spectroscopy the radiation is absorbed by the molecule and depends upon the change in dipole moment, Raman spectroscopy is a two-photon process that involves the inelastic scattering of the incident radiation and depends upon the change in the polarizability. Scattered light from a molecule can be categorized as either Rayleigh, elastically, or Raman, inelastically, scattered light. Raman scattered light can be further differentiated as either Stokes or Anti-Stokes emission. The absorption and emission of the different types of radiative processes used in vibrational spectroscopy are represented in Figure 3.
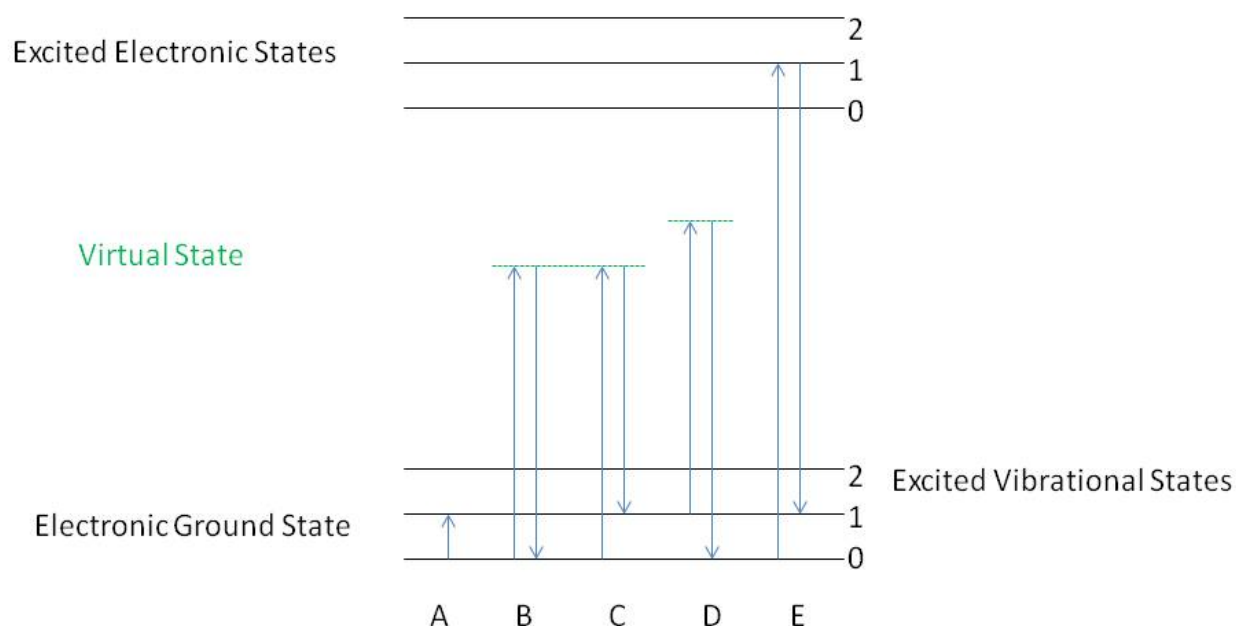
Figure 3. A diagram comparing IR absorption (A) and Rayleigh Scattering (B) with the different forms of Raman Scattering: (C) Stokes Raman, (D) Anti-Stokes Raman, (E) Resonance Raman

The majority of the scattered light is due to Rayleigh scattering in which after being excited to an intermediate, virtual state, the molecule returns to the same vibrational state in the electronic ground state. The scattered light involved in this process is of the same energy as the incident light and is the elastically scattered Rayleigh light. The process of Raman scattering occurs when a molecule is excited from its ground electronic state to a virtual state and returns to its ground electronic state, but a different vibrational state. As noted in Figure 3, the Raman process has two different ground-to-virtual state processes that can occur. The first, Stokes scattering, is more common and occurs when the molecule is excited from its ground vibrational and electronic state to a virtual state and returns to the ground electronic state in a

higher vibrational state. When this occurs, the energy of the scattered light is lower, and therefore the frequency of the scattered light is lower than that of the incident light. This difference in frequency can give us a great deal of information about the molecule as its frequency is dependent upon the difference in energy between the two vibrational levels. The other type of non-resonant Raman scattering that involves scattered light at a higher frequency than that of the incident light is called Anti-Stokes scattering (Fig. 3D). This process occurs when a smaller fraction of light, than that involved in Stokes scattering, interacts with a molecule so that after being excited to a virtual state, it returns to a lower vibrational level of the ground electronic state than where it was before.

The relative intensities of the Rayleigh, Stokes, and Anti-Stokes scattered light can be directly related to the probability of finding a molecule in specific electronic and vibrational states. The Boltzmann constant is the key factor in the ratio of Stokes to Rayleigh scattering, the Rayleigh scattering being more intense. The ratio of the number of molecules that undergo Stokes scattering, as compared to those undergoing Anti-Stokes scattering, is dependent on the number of molecules that are initially in a state higher than the ground vibrational state. This leads to much lower intensity signals, which for high frequency vibrations, can be of the order of several magnitudes for Anti-Stokes scattering, especially at room temperature where a very small portion of the molecules are not in the ground vibrational state.

2.1   Resonance Raman Spectroscopy

Resonance Raman scattering (Fig. 3E) occurs when the energy difference between the ground and excited electronic states is similar to that of the incident light. By "tuning-in" to these

electronic transitions, we can see a change in the intensity of some bands by several orders of magnitude when compared to normal Raman scattering. The specific excitation wavelengths that can give us this resonance enhancement as great as a factor of 10^8, correspond with the molecule's electronic absorption frequencies [59,60]. All three types of scattering, Rayleigh, Stokes, and Anti-Stokes still occur in resonance Raman, the main difference is that the molecule goes to an excited electronic state instead of a virtual state.

Ultraviolet resonance Raman (UVRR) spectroscopy utilizes deep UV light as an excitation source for select vibrations. Utilizing excitation around 200 nm to tune-into the π→π* electronic transition of the peptide amide bond, occurring between 180-215 nm, selectively enhances specific vibrations of the peptide amide bond[61]. By using incident light in this region, the UVRR spectrum is dominated by amide vibrations that are sensitive to bond angles, solvent exposure, and hydrogen bonding.

The key amide vibrations that arise from UVRR spectroscopy that utilizes the π→π* electronic transition are well known (Figure 4). The amide I (AmI) vibration is mainly a C=O stretch and is known to be sensitive to the hydrogen bonding that occurs at the amide bond. The amide II (AmII) vibration is a C-N stretch with N-H out-of-plane bend and C-C stretch. The amide III (AmIII) vibration is very complex and composed of C-N stretch with N-H in-plane bend and C-C stretch, and has been found to be a sensitive marker of peptide secondary structure[62]. The C_α-H bend vibration, a C_α-H symmetric bend with C-C_α stretch, is not always seen depending on the conformation of the amide bond.

Amide I

Amide II

Amide III

C_α-H bending
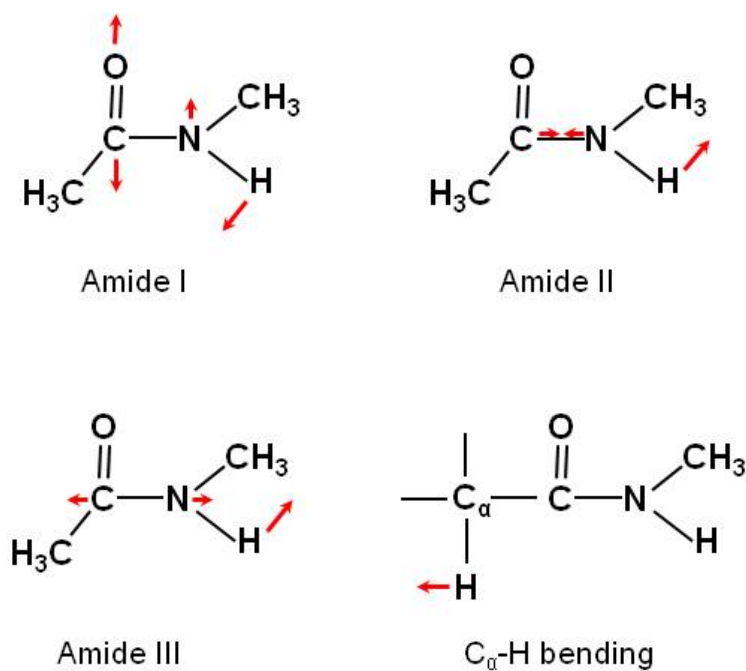
Figure 4. Atomic motions of the enhanced amide bands.

With much innovation and development by the Asher group, UVRR spectroscopy has become a technique that is unparalleled for the determination of protein and peptide structure. Through the use of the key amide vibrations, the group has developed spectral markers for peptide secondary structure[61]. UVRR spectroscopy can also provide kinetic information of structural changes with temporal resolution as low as 3 nsec[63]. The ability to obtain both structural and kinetic data from the same experiment makes UVRR spectroscopy a great tool to study changes of any amide containing molecules.

3.0 Monitoring the VPT of PNIPAM by C-H Stretch Frequency

3.1 Introduction

One of the key factors in understanding the VPT of PNIPAM is to gain a clear molecular picture of the solvation of the hydrophobic isopropyl moiety of the monomer unit (Fig. 5), as it is expected to be in different environments at temperatures above and below the LCST. It has been shown that the C-H stretch vibration is sensitive to hydrogen bonding and solvation, especially the asymmetric stretch of the methyl group[47]. The greater the number of solvating waters around a methyl group, the higher the frequency of the C-H stretching vibration[64]. Through UVRR spectroscopy we can gain a clear picture of the changes that the amide moiety undergoes through the VPT, but the C-H stretch region in UVRRS is complicated by amide overtones so visible non-resonant Raman is utilized.
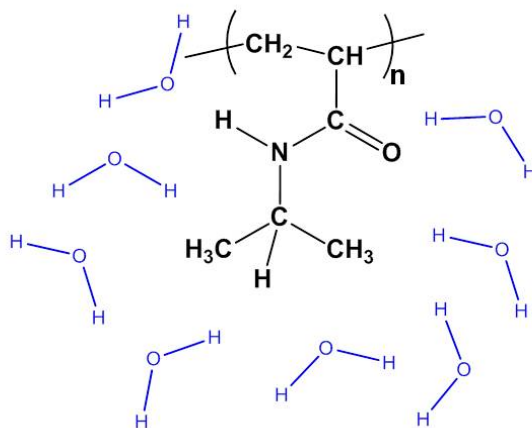

Figure 5. Molecular structure of a PNIPAM monomer unit solvated by water molecules.

The rationalization for the change in C-H stretch frequency due to hydrogen bonding has been studied and debated for many years, and there is still no clear answer on exactly how the C-H participates in hydrogen bonding. In the case of standard hydrogen bonding, X-H•••Y, we expect to see a weakening of the X-H bond leading to a downshift in the X-H stretch frequency. However, improper, or blue-shifted, hydrogen bonds have been found in the case of liquid phase C-H•••O type hydrogen bonding[65]. These blue-shifted hydrogen bonds have a decrease in the C-H bond length rather than the lengthening of the bond that we see in typical amide-water hydrogen bonding. This difference in bond length is found to be the major difference between the typical O-H•••O and the C-H•••O hydrogen bonds. Both types cause changes in electron density and are sensitive to changes from equilibrium geometry[66]. Although the origin of the improper, or blue-shifted, hydrogen bond is still being debated, the phenomenon is well accepted[65-69].

Although the PNIPAM microspheres are cross-linked and have a co-monomer (see experimental

section 3.2.1), NIPAM maintains a majority mole fraction of the hydrogel microsphere. The

visible Raman spectra have some contribution in the low frequency section of the C-H stretch

region from the backbone or co-monomers and can be seen in Figure 6. The four distinct C-H

stretch vibrational bands appear at similar frequencies, and with the structural similarities, the

same band assignment can be used for the isopropanol and PNIPAM C-H stretch Raman bands.

The highest frequency band is the most void of any contribution and can be definitively

assigned to the antisymmetric C-H of the methyl groups[70].
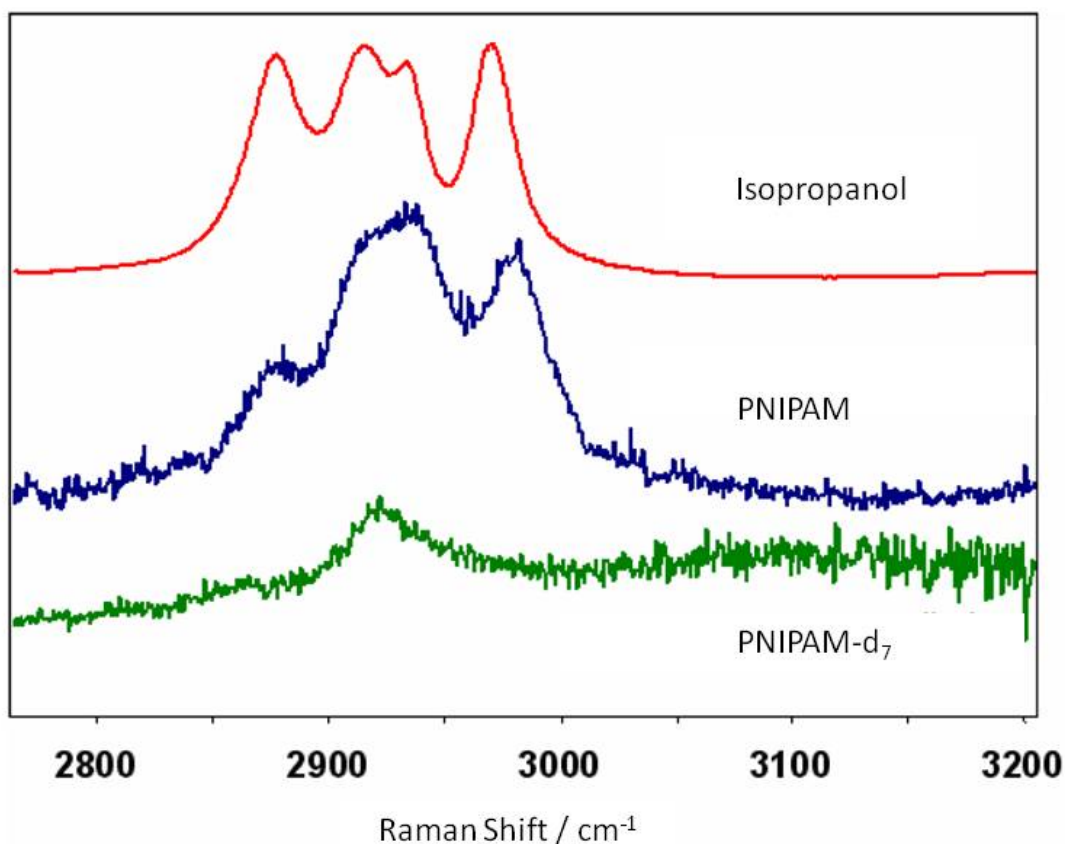

Figure 6. 488 nm excited Raman spectra of neat isopropanol, PNIPAM, and PNIPAM-d_7 showing that the C-H stretch region of PNIPAM is dominated by the vibrational bands of the isopropyl moiety. Adapted from reference [1].

3.2   Experimental Methods

3.2.1   Sample preparation

All solutions were made with D_2O (99.9 % D). PNIPAM microspheres were synthesized via

dispersion polymerization using 2.1790 g NIPAM (Aldrich), 0.0379 g 2-acrylamido-2-methyl-1-

propane-sulfonic acid (ionic co-monomer, Aldrich), 0.1155 g N,N'-methylenenbisacrylamide

(cross-linker, Fulka), 0.0578 g Sodium dodecyl sulfate (surfactant, Aldrich), and 0.1385 g

Ammonium persulfate (initiator, Aldrich) in 0.1 mM $NaHCO_3$. The solution was reacted at 70 °C

for 4 hours with stirring. The particle solution was then filtered with glass wool and placed on a

spinner with AG 501-X8 (D) ion exchange resin (BioRad) for 3 weeks before use. Particle size

was measured by dynamic light scattering using a Brookhaven Instruments ZetaPALS Zeta

Potential Analyzer.

The Raman spectra from the particles will be dominated by that of the NIPAM monomer and its

isopropyl moiety. The particles that were synthesized in D_2O for this experiment, assuming that

all monomers were incorporated equally, are 93.4 wt. %, 88.19 mol % NIPAM. The iPrOH

concentration for this experiment is 10x that of the NIPAM percent in D_2O. The 10x

concentrated solution was used to have an increased intensity of the C-H stretching vibrations

with respect to the O-D stretch for better signal intensity.

3.2.2   Visible Raman Instrumentation

Horiba Xplora with LabSpec5 software was used for collection of visible Raman spectra. 532 nm

excitation with 50 % laser filter and 1200T grating, 10x magnification objective, with the

spectral slit set and the confocal hole both set to 100 was used. Exposure time for the PNIPAM

sample was 3 accumulations of 180 sec and 3 accumulations of 120 sec was used for the iPrOH

sample at each temperature.

Sample temperature was controlled by a home-built sample cell that was connected to a

circulating water bath. The sample volume was ~1 mL, and a high quality quartz cover slip was

placed on top of the sample well to prevent evaporation. All samples were equilibrated at new

temperatures for 10 minutes before taking spectra.

3.3   Results and Discussion

The spectral region of PNIPAM aqueous solutions is dominated by the O-D and O-H stretch,

even with a sample as concentrated as 2.1 wt %. The spectra of the PNIPAM at temperatures

from 10-50 °C can be seen in Figure 7. The change in temperature can be seen by the

characteristic change in band shape of the O-D stretch. The C-H stretch region, 2800-3000 cm^{-1},

does not show a significant change in either band shape or position when examining the
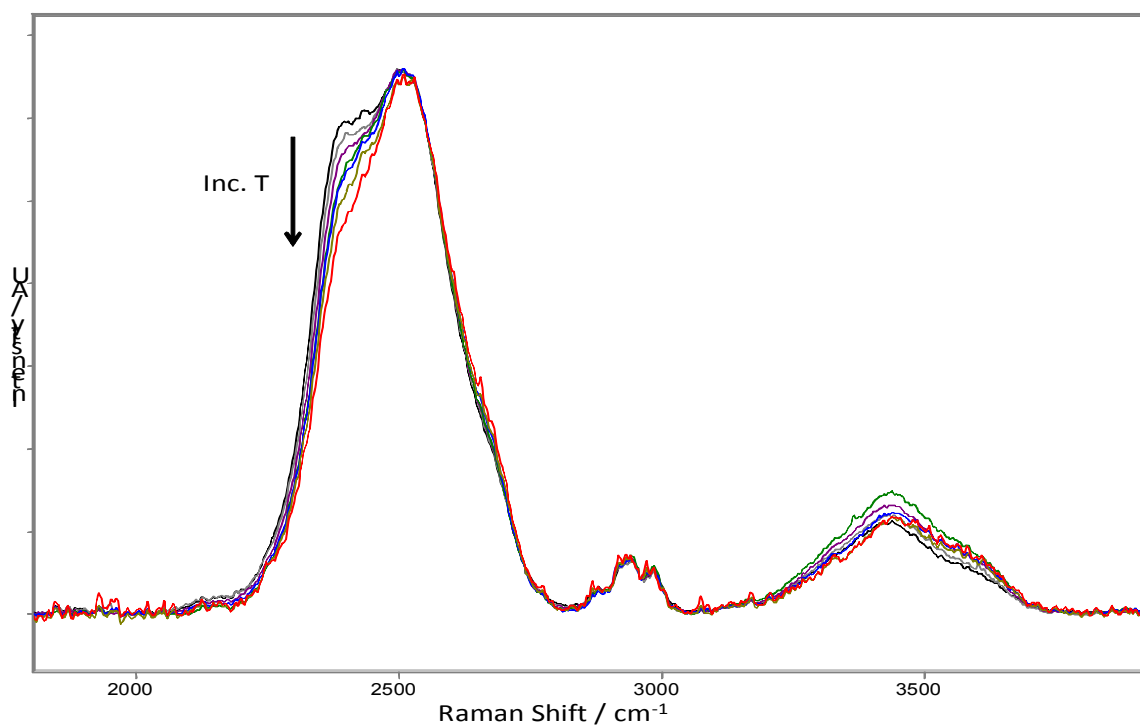
spectra in its entirety.

Figure 7. 532 nm excited Raman Spectra of PNIPAM in D_2O from 15 – 50 °C. The change in temperature can be observed with the change in band shape of the D_2O (~2500 cm^{-1}).

Upon deconvolution of the spectra as a mix of Gaussian and Lorentzian bands, we can see that

the frequencies of the four components of the C-H stretch region are decreasing as the

temperature of the solution increases. This behavior is consistent with previous studies

indicating a downshift in C-H stretching frequency as a reliable indication of dehydration, as

discussed in the previous section. The use of four bands in this region is consistent with the

fitting and previous assignment of the isopropyl group[70,71]. The peak fit and the band

assignments can be seen in Figure 8 and Table 1.
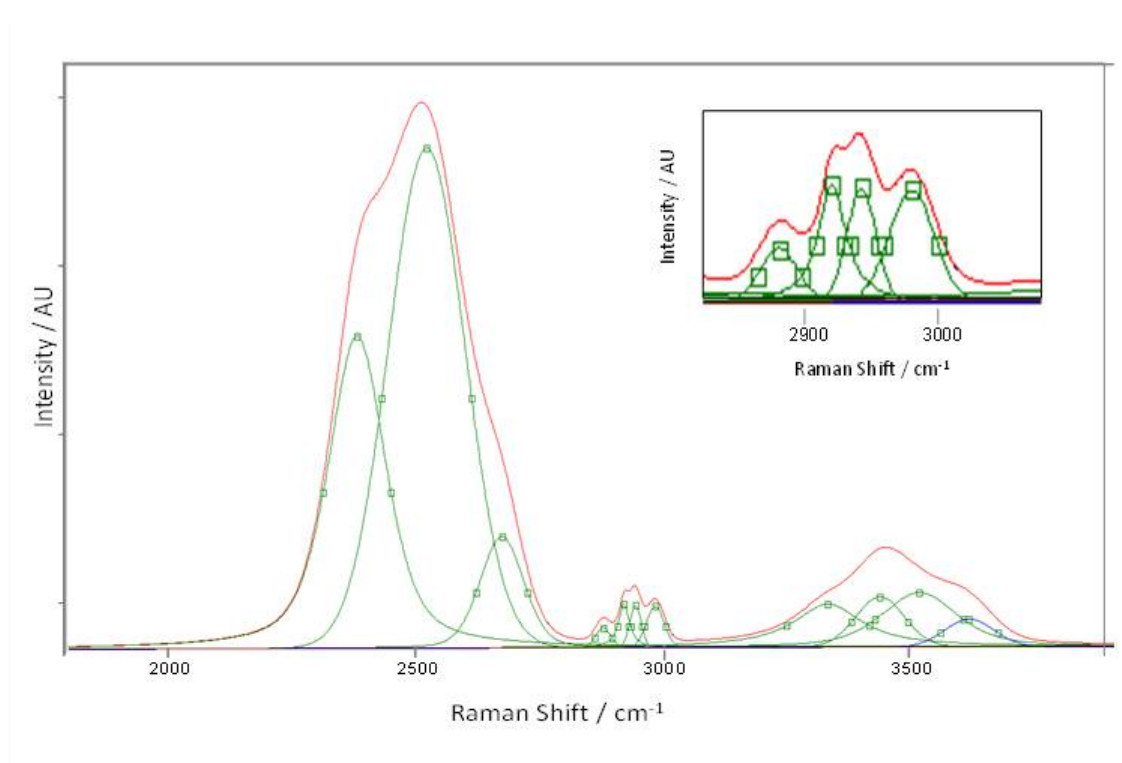

Figure 8. 532 nm excited Raman Spectrum of PNIPAM in D_2O at 35 °C. The spectrum was fitted with a minimum sum of mixed Gaussian and Lorentzian bands. Insert is the C-H stretch region that was decomposed into four bands.

The four CHs bands have been assigned to:

	Raman Shift in iPrOH (cm^{-1})	Tentative Assignment
CHs 1	2882	C-H stretch
CHs 2	2921	
CHs 3	2943	CH$_3$ stretch
CHs 4	2982	CH$_3$ antisymmetric stretch

Table 1. Band assignments for C-H stretch region of aqueous PNIPAM solution.

The lower frequency bands have some discrepancy in their assignment and may have contributions from not only the isopropyl moiety of the NIPAM monomer, but also small contributions from co-monomers and the backbone of the polymer. The changes in the frequency of the four vibrations over the VPT can be seen in Figure 9.
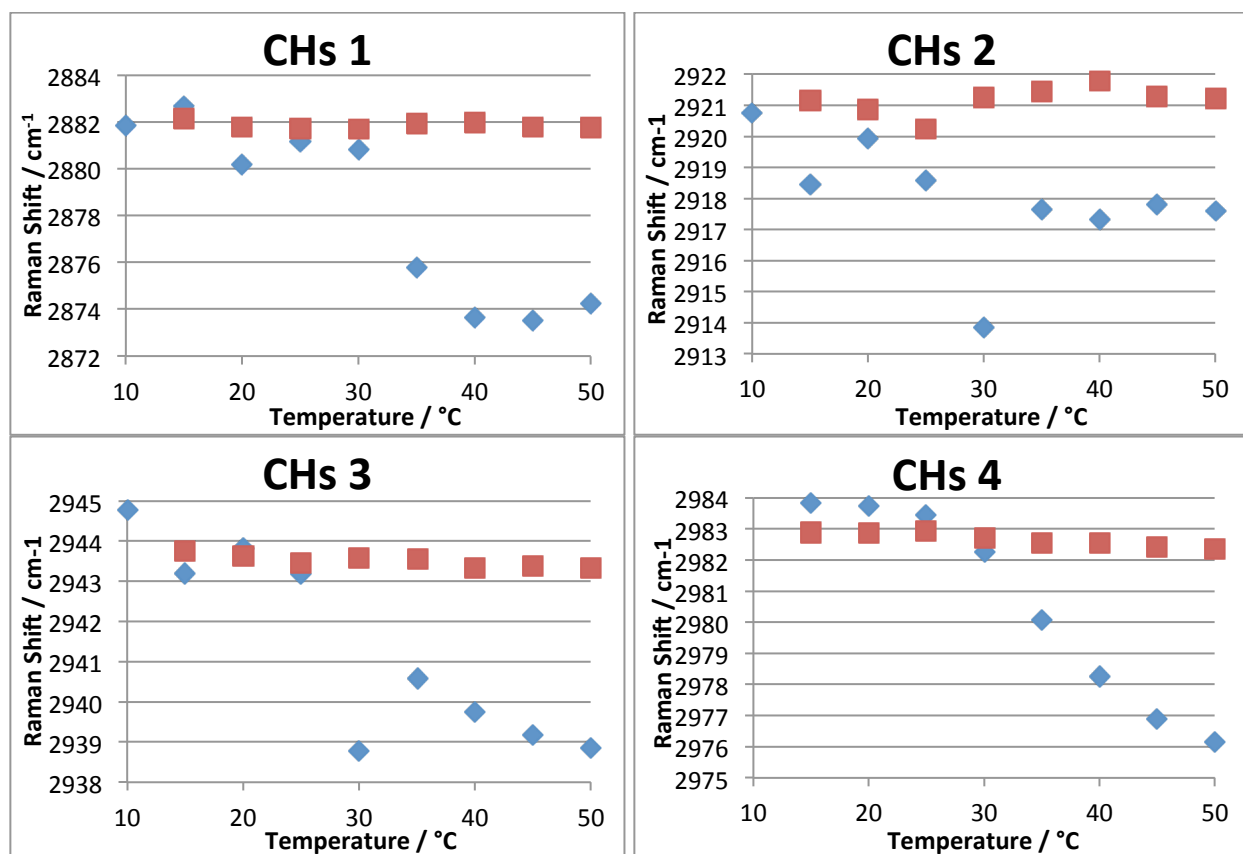
Figure 9. The frequency shifts in the four spectral bands of PNIPAM (blue) and Isopropanol (red) in D2O at temperatures over the VPT.

■ : iPrOH in D_2O ◆ : PNIPAM Particles in D_2O

The graphs in Figure 9 indicate that the change in the C-H stretching frequencies that are observed in the Raman Spectra of PNIPAM particles is predominantly due to the change in hydration of the isopropyl side chain and not due to a change in temperature. The isopropanol in D_2O solution was monitored to ensure that all spectral trends were as a result of the PNIPAM VPT and subsequent dehydration, and not a result of only temperature change.

The magnitude of the frequency shift of CHs 2 is the smallest at only 4 cm^{-1}, indicating that it is either the least sensitive to the dehydration or derives from a vibration that is not experiencing large changes in its hydrogen bonding. CHs 1 and CHs 4 have frequency shifts of 8-9 cm^{-1}, while CHs 3 has a shift of 6 cm^{-1}. The most sensitive vibrations seem to be that of CHs 1 deriving from the C-H of the isopropyl moiety and CHs 4 of its methyl groups. Due to the possibility of contributions from co-monomers or backbone C-H stretch vibrations, the best marker for the change in the hydration of the isopropyl moiety is CHs 4, the antisymmertic C-H stretch of the methyl groups.
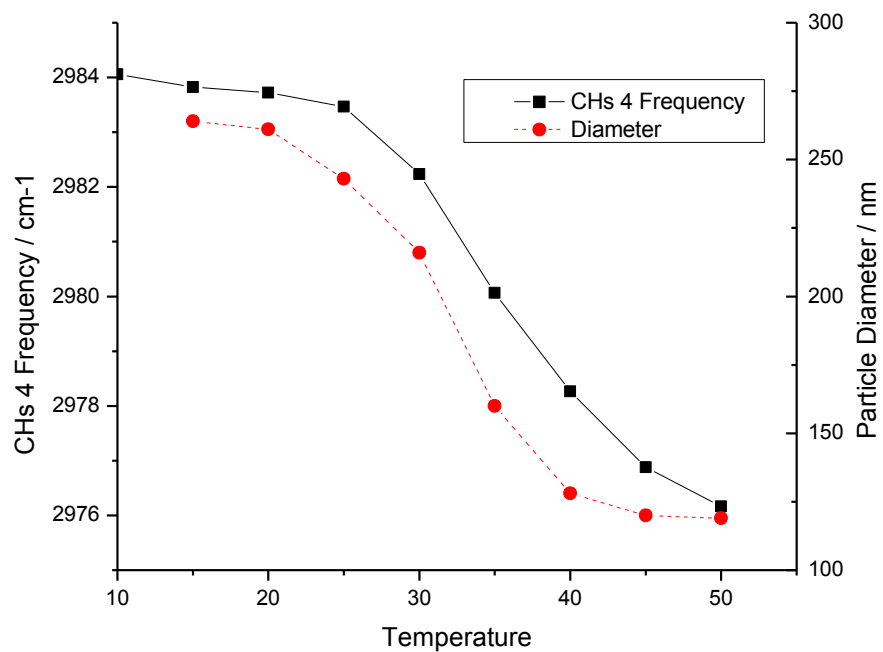

Figure 10. Graph of the shift in the antisymmertic C-H stretch of the methyl groups (left axis) and the particle diameter (right axis) over the VPT.

The change in Raman shift of the four C-H stretch vibrations when plotted against temperature is very similar in shape to that of the particle diameter with respect to temperature (Fig. 10). The decrease in diameter over 15-50 °C (264 to 119 nm diameter) causes approximately 2.9×10^8 molecules of water to be excluded from the polymer microsphere. This is accompanied by a shift in the CHs 4 of 8 cm^{-1} (2684 to 2076 cm^{-1} from 15-50 °C).
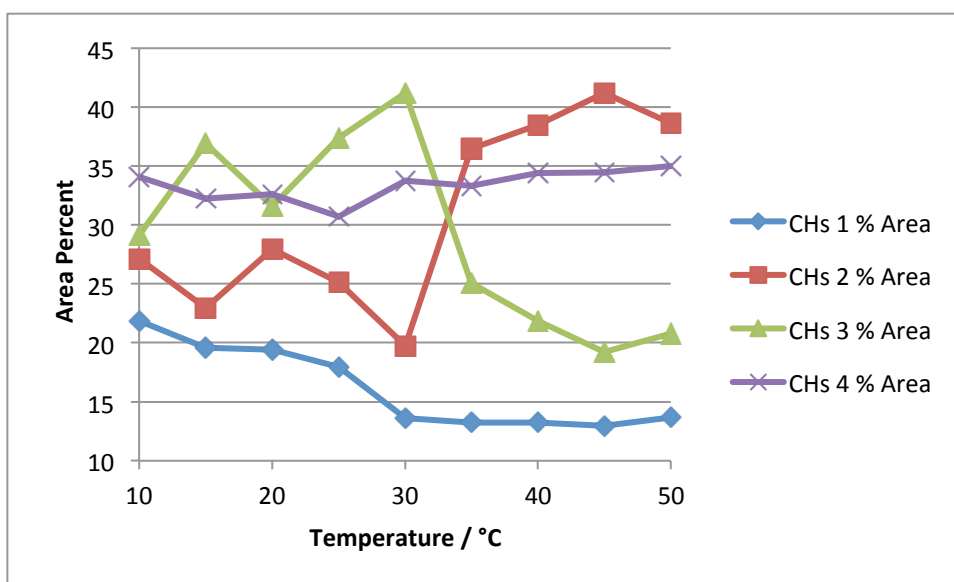
Figure 11. The relative percent area of the four C-H stretch vibrations of PNIPAM microspheres in D$_2$O.

When examining the percent area of each band, it was discovered that the CHs 2 and CHs 3 bands had a distinct changes in their relative areas. The CHs 2 becomes more prominent, and the CHs 3 less, after temperature is above the LCST. Over the temperature range, the CHs 1 of the central carbon decreases in relative area with the most significant drop occurring at temperatures just below the LCST. This could be a good indication that the C-H of the isopropyl

side chain is experiencing a change in environment and hydrogen bonding before the methyl groups. This would indicate that the loss of hydrogen-bonded water at the amide is disturbing the hydration shell of the hydrophobic sidechain, and possibly triggering the bulk dehydration of the isopropyl group.

3.4   Future Work: Examination of the Kinetics of the VPT Using a Visible Excitation Temperature-jump

After noting the significant change in the C-H stretching region of PNIPAM of steady-state temperature-dependent Raman spectra, it would be useful to have kinetic data on the dehydration of the isopropyl groups. To do this, a visible Raman temperature jump experiment could be performed. The 532 nm output of a Nd:YAG laser could produce the probe pulse subsequent to the IR heating pulse. The D_2O stretch region can be used to monitor the magnitude of the temperature change, and the visible excitation will decrease the contributions of the amide vibrational overtones that can complicate this region in the UVRR spectra. By examining the delay times at which the C-H stretch region begins to change, we can further understand the order of dehydration of the PNIPAM monomers.

A significant complication with this method in that the stream will have to be ~100 μm thick or visible absorbers will need to be used to ensure that the probe pulse is only sampling the region of the stream that is heated from the absorbed IR pulse.

4.0   Low Concentration ClO$_4^-$ Induces Aggregation in PNIPAM Microspheres

4.1   Introduction

The multitude of studies on PNIPAM and other stimuli-responsive polymer microgels have led to the discovery of some interesting phenomena that need to be further explored. It is known that that particles can swell and collapse based on a change in solvent composition and the ionic strength of the bulk water in the particle. It has been demonstrated that when no added electrolyte is present, the screening effect of the counter-ions helps to stabilize the expanded particle. On the contrary, the particles collapse when the PNIPAM microgels are in the presence of high salt concentrations[72]. The further addition of either heat or salt can induce aggregation of the microgel particles.

Extensive work has been done on the studies of salt-induced homoaggregation of microgel particles mostly utilizing light scattering, electrophoresis, and viscometry[72-74]. A comprehensive study of the effect of various ions on the collapse and aggregation was done by Daly and Saunders and showed that at room temperature, a PNIPAM microgel particle can remain swollen as long as the concentration of the added salt does not go above 0.5 M. They also demonstrated that anions have a greater effect on the aggregation as compared cations in the solution. The effect of the anion on the aggregations tends to follow the lyotropic series where the cations did not have an observable trend, indicating that it may be a result of factors other than direct hydration of the cation by water molecules. The anions that were found to have the

greatest effect on causing the aggregation where those with the highest charge density and polarizability[73].

4.2   Experimental Methods

4.2.1   Sample Preparation

PNIPAM microspheres were made via dispersion polymerization using 1.4174 g NIPAM, 0.0248 g 2-acrylamido-2-methyl-1-propane-sulfonic acid (ionic co-monomer, Aldrich), 0.0667 g N,N'-methylenenbisacrylamide (cross-linker, Fulka), 0.0370 g Sodium dodecyl sulfate (surfactant, Aldrich), and 0.0891 g Ammonium persulfate (initiator, Aldrich) in 0.1 mM NaHCO$_3$ in 18 MΩ DI water. The mixture was reacted for 4 hours at 70 °C with stirring. The solution was then filtered through glass wool and dialyzed against DI water for 3 weeks using regenerated cellulose tubing (Fisherbrand, 12,000-14,000 MWCO). The particle solution was then stored with AG 501-X8 (D) ion exchange resin (BioRad) to continue to remove any free ions left in solution. Particle size was measured by dynamic light scattering using a Brookhaven Instruments ZetaPALS Zeta Potential Analyzer.

The solutions to be studied were 0.25 wt % PNIPAM in either DI water or 0.05 M NaClO$_4$.

4.2.2   UVRR Instrumentation and Set-up

204 nm excitation was achieved using a 1 kHz repetition rate Ti:sapphire laser from Photonics Industries with an average energy of 1.3 µJ per pulse and a pulse width (fwhm) of 26 ns. The spectra were collected on a home-built UVRR spectrometer[75].

4.3   Results and Discussion

The aggregation process that the PNIPAM microspheres undergo when above the LCST and in the presence of 0.05 M NaClO$_4$ was monitored with dynamic light scattering (DLS). The PNIPAM microspheres in the ClO$_4^-$ solution are slightly smaller at the lower temperatures, before aggregation is induced. At 20 °C the particles in DI water are 180 nm where the particles in 0.05 M ClO$_4^-$ are 168 nm at 30 °C the particles are 156 and 133 nm respectively. As the solution goes above the LCST the aggregation process is evident. At 35 °C the difference in particle diameter of the microspheres in ClO$_4^-$ is recorded as nearly 5 times that of the microspheres in DI water. The process is reversible as the particles in ClO$_4^-$ return to a diameter of less than 200 nm below the LCST.
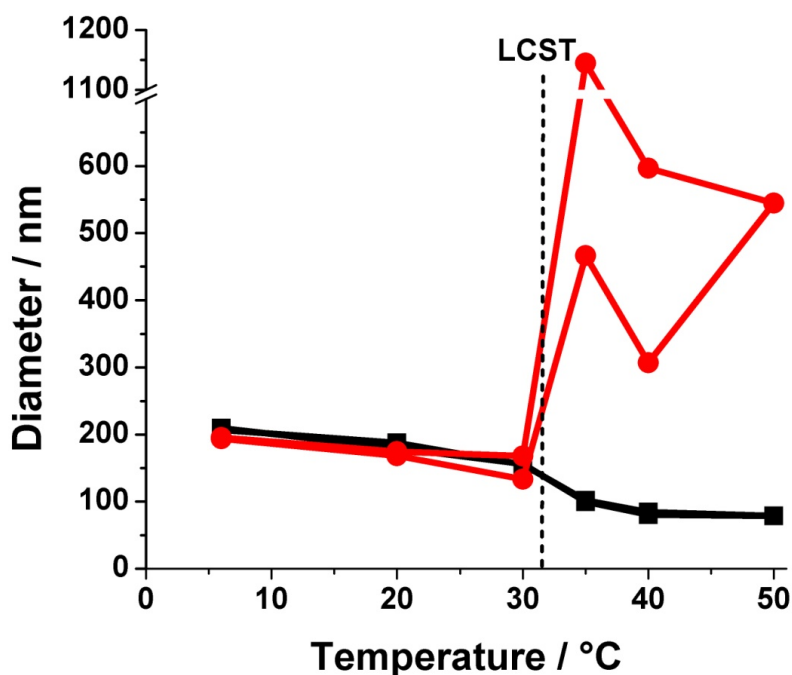

Figure 12. DLS measurements following the reversible aggregation of 0.25 wt. % PNIPAM microspheres (red) and the VPT of 0.25 wt. % PNIAM microspheres in DI water (black).
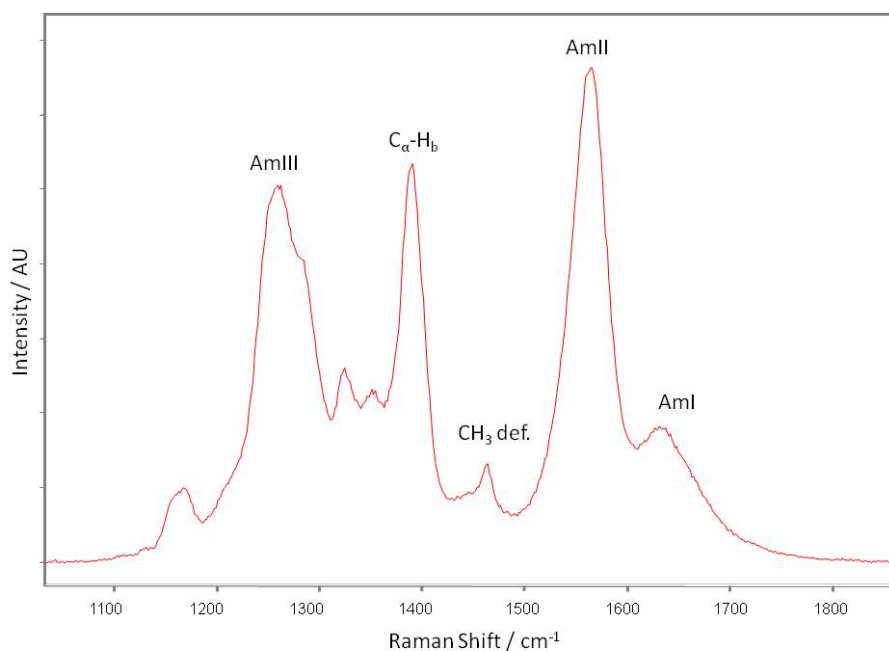
Figure 13. The 204 nm excited UVRR spectra indicating the enhanced amide vibrations of PNIPAM and the CH_3 deformation band at 30 °C.

Steady state, 204 nm excited UVRR spectra of PNIPAM microspheres in DI water from 4 to 40 °C. Spectra were normalized to the intensity at 1460 cm^{-1}, the isopropyl group's CH_3 deformation band. The amide region of the UVRR spectra of PNIPAM strongly resembles that of a peptide, with the characteristic bands present that are described in Figure 4. The strong AmIII band is located centered at 1259 cm^{-1} with two shoulders at ~1230 and 1282 cm^{-1}. There are two additional, weaker AmIII bands appearing at 1342 and 1352 cm^{-1}. It is likely that the multiple AmII bands are due to a coupling with the vibrations of the isopropyl group. The C_α-H bending vibration is seen strongly at 1389 cm^{-1}. The AmII band is located at 1564 cm^{-1} and the AmI is a broad band observed at 1631 cm^{-1}.

4.3.1 Temperature Dependence of PNIPAM

Upon heating from 4-40 °C, the AmII vibrational band downshifts from 1568 to 1560 cm^{-1} and decreases in intensity. The AmI region shows the opposite trend with an up shift in frequency from 1624 to 1643 cm^{-1} and an increase in intensity as the solution temperature increases from 4 to 40 °C. The AmI region can be decomposed into three Gaussian bands (Fig. 15).
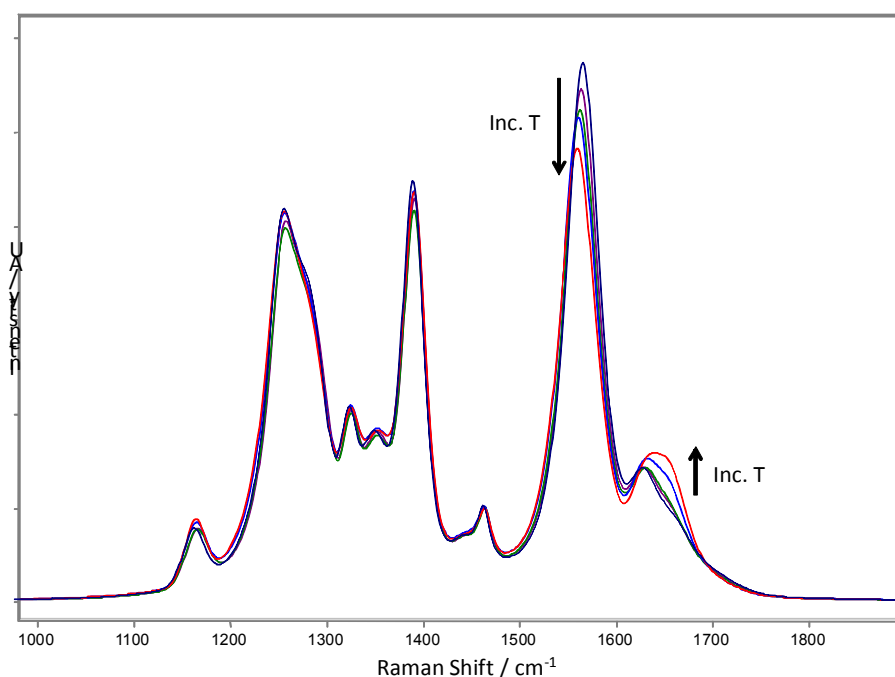
Figure 14. The amide region of the 204 nm excited UVRR spectra of PNIPAM in DI water over the VPT, 4-40 °C. The greatest changes occur in the AmII, ~1565 cm^{-1}, and the AmI, ~1635 cm^{-1}. The spectra were normalized to the intensity of the CH$_3$ deformation band at ~1460 cm^{-1}.

Figure 15. The 204 nm excited URVV spectra of PNIPAM at 4 and 40 °C. The spectra were fitted to a mix of Gaussian and Lorentzian bands, with Gaussian bands being used for the AmI region.

The band centered at ~1625 cm^{-1} derives from the amide being fully hydrated, while the ~1690 cm^{-1} band is likely from completely dehydrated amides. The vibration a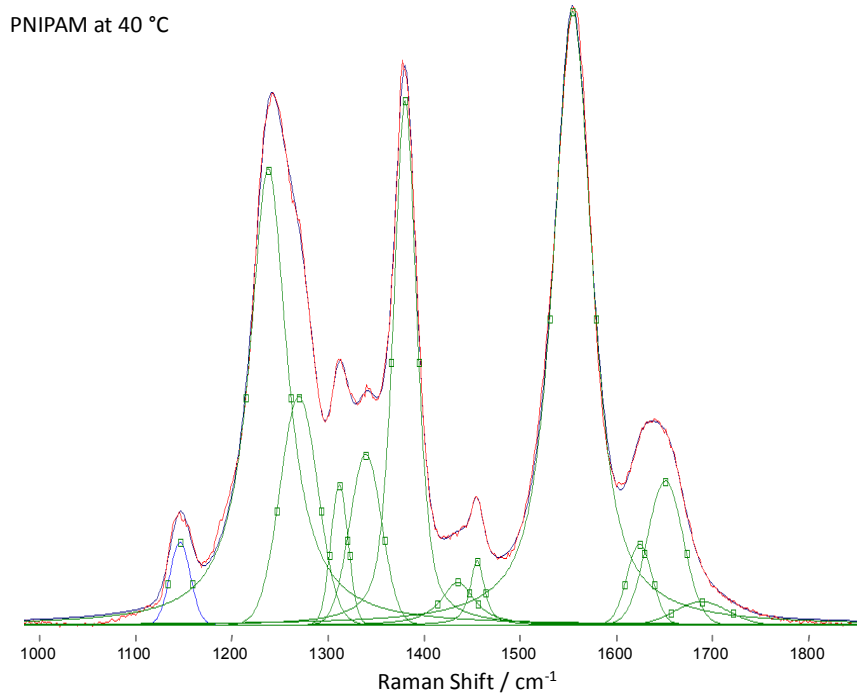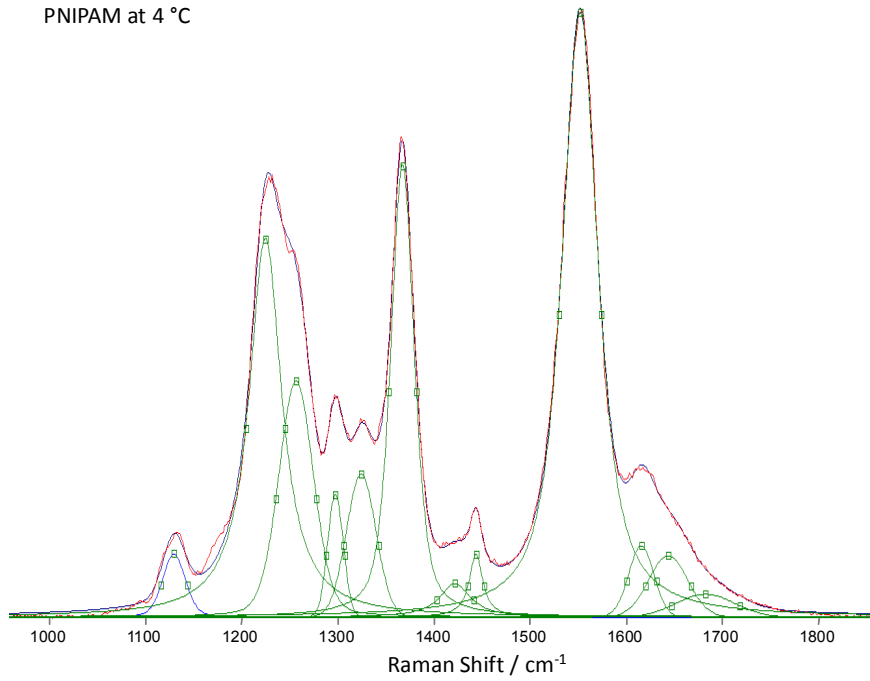t ~ 1650 cm^{-1} is thought to be a partially dehydrated amide with only 2 waters involved in hydrogen bonding, one each at the C=O and N-H sites, rather than the 3 waters involved in the fully hydrated amide. The presence of all three AmI bands can be seen at 4 °C. The 40 °C spectrum shows the dominant vibration to be that partially dehydrated amide. The changes in relative percent area of the three AmI components as the PNIPAM goes through the VPT are seen in Figure 16.
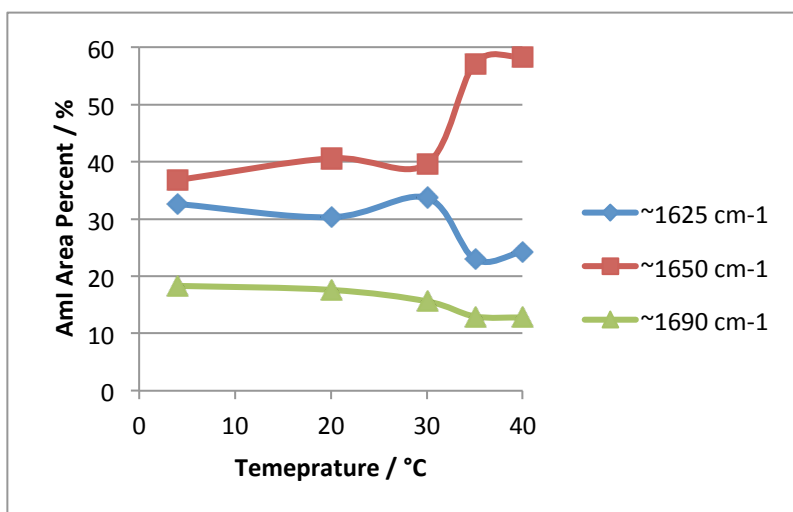

Figure 16. The relative percent area of the three AmI vibrational bands between 4 and 40 °C of 0.25 % weight PNIPAM solution in DI water. The values are from 204 nm excited UVRR spectra, decomposed with a mix of Gaussian and Lorentzian bands.

PNIPAM microgel spheres in DI water show a distinctive transition in the AmI region as the temperature of the solution is brought above the LCST. The 1650 cm^{-1} band that indicates a partially hydrated amide bond has a significant increase in area, while the 1625 cm^{-1} band shows a 10 % decrease in area percent of the AmI. This indicates that the Amide moiety is no longer involved in hydrogen bonding with the solvating water molecules to the degree that it was before and has most likely lost a water molecule involved in hydrogen bonding to the N-H site.

4.3.2   Raman Interpretation of PNIPAM Aggregation in 0.05 M NaClO$_4$

When a salt is introduced into the aqueous PNIPAM system, we can see that there are distinct changes in the Raman spectra as well as visible aggregation in the solution above 35 °C. The UVRR spectra collected from 4-40 °C can be seen in Figure 17. The figure shows the spectra normalized to the intensity of the ClO$_4^-$ band at 932 cm^{-1}. By normalizing to this band, we can see that the intensity of the spectra are significantly altered once the aggregation occurs due to the lack of PNIPAM microspheres traveling through the pump and sample stream. However, the changes to the AmI and AmII vibrations band shape and frequency indicate that changes in the hydrogen bonding are still occurring.
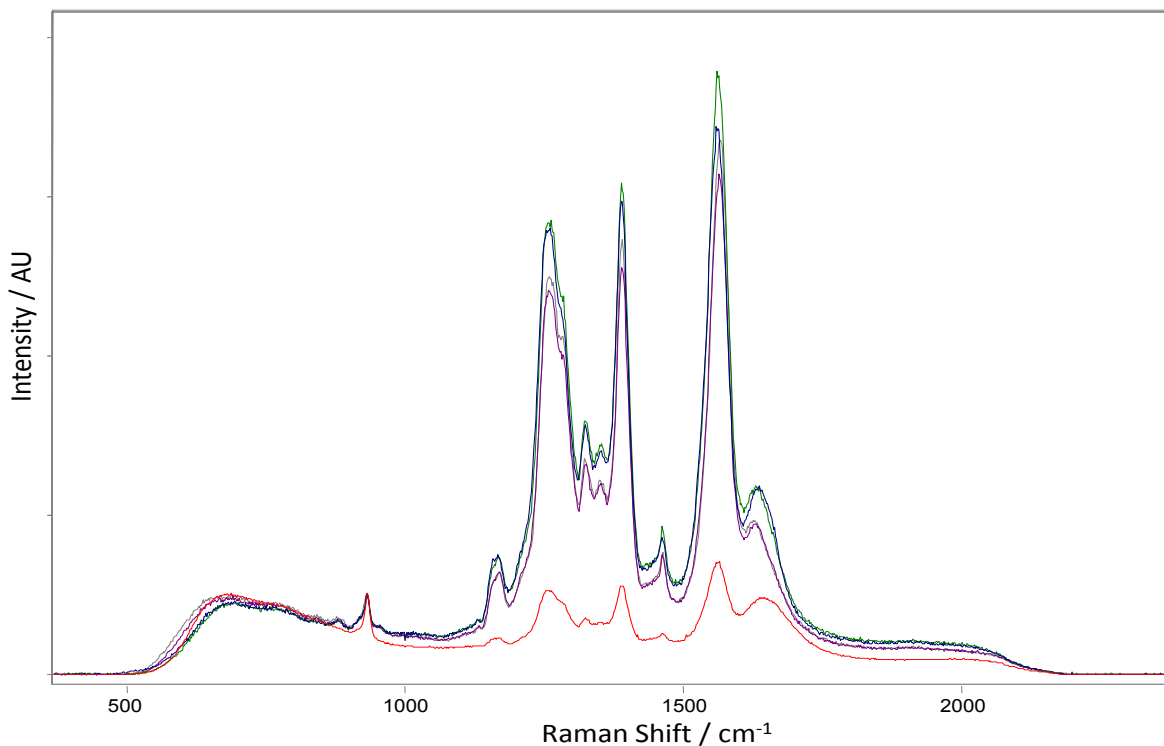
Figure 17. 204 nm excited UVRR spectra of 0.25% PNIPAM in 0.05 M NaClO$_4$ normalized to 932 cm^{-1} ClO$_4^-$ band intensity. The red spectrum is from 40 °C and indicates a large loss of PNIPAM in the sample stream with the decrease in relative intensity of the PNIPAM vibrations to that of the water and ClO$_4^-$.

For spectral analysis, the PNIPAM in 0.05 M NaClO$_4$ spectra were normalized to the intensity of the CH$_3$ deformation band at ~1460 cm^{-1}, the same was done for the PNIPAM in DI water. Upon examining the percent area of these three components of the AmI vibration (Fig. 18), it was noted that above the LCST, where particle aggregation has been seen in the sample, the fully dehydrated AmI vibration (~1690 cm^{-1}) dominates. This is contrary to the behavior that is seen in the particle solutions in which ClO$_4^-$ is not present. The ~1625 cm^{-1}, fully hydrated amide vibrational band is seen consistently to be at a lower percent area than in the pure DI water sample. The partially dehydrated AmI band at ~1650 cm^{-1} indicates that the amide is more

hydrogen bonded until the above LCST at which point the agreggation begins to dominate. As

the agreggation continues, we see a sharp incease in the area of the ~1690 cm^{-1} band that

indicates a fully dehydrated amide is more abundant.
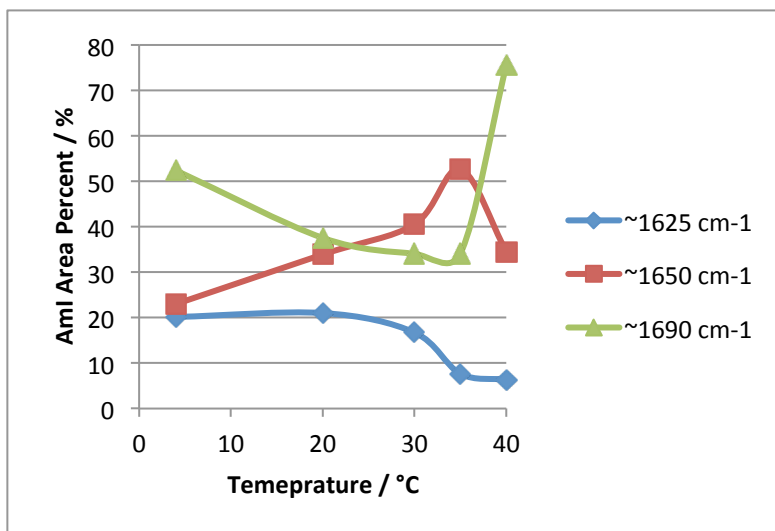
Figure 18. The relative percent area of the three AmI vibrational bands between 4 and 40 °C of
0.25 % wt. PNIPAM solution in 0.05 M NaClO$_4$. The values are from 204 nm excited UVRR spectra,
decomposed with a mix of Gaussian and Lorentzian bands.

The AmII vibration is also a marker for the hydrogen bonding environment of the amide bond.

A downshift of the AmII vibration is a spectral marker of the weakening or loss of amide-water

hydrogen bond[50,63]. In the spectra of both the microspheres in DI water and 0.05 M NaClO$_4$, as

the temperature of the solution increases towards the LCST, we see a downshift in the

frequency of the AmII vibration. Above the LCST, when aggregation was present in the salt

solution of PNIPAM, we see an upshift in the frequency of the AmII (Fig. 19). This upshift would

indicate that there is a weakening or lengthening of the amide bond. This could be caused by the formation of intramolecular hydrogen bonding rather than that of the amide-water, intermolecular hydrogen bonding.
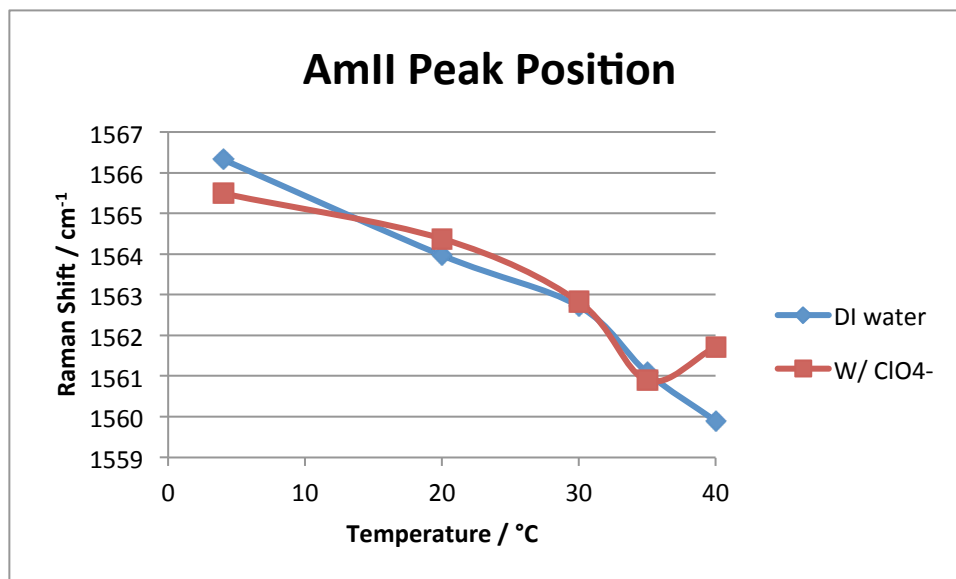
Figure 19. The change in Raman shift of the AmII vibration across the VPT of PNIPAM microspheres in both DI water and 0.05 M $NaClO_4$. The microspheres begin to aggregate above ~32 °C.

The upshift in the AmII is contradictory to what is seen in the AmI vibration as the AmI frequency shift and change in area indicates a loss of hydrogen bonding in the aggregation process, while the AmII indicates an increase. Further work will need to be done to determine the exact cause of the weakening of the amide bond indicated by the upshift of the AmII vibration.

From the changes in the UVRR spectra collected in the presence of the $NaClO_4$ as compared to those from the PNIPAM in DI water, we can see that the presence of the ions has a great effect on the particles behavior above the LCST. The thought is that there is a screening effect that disrupts the repulsion between ion comonomer units that typically aids in stabilizing the expanded particles. Along with this screening effect, the ClO_4^- can compete with the amides for hydrating water molecules. The spectra indicate that the ClO_4^- succeed at disrupting the amide-water hydrogen bonding that occurs under standard conditions.

4.4   Future Work

To further examine the structure of these aggregates and their hydrogen bonding, a different sample technique could be employed. The samples in this experiment were circulated through a temperature controlled peristaltic pump. To better examine the aggregates, the use of either a spinning cell or a microscope could be employed. Previous experiments done by the Asher group have utilized a spinning NMR tube that would force the larger particles/aggregates against the tube walls to be sampled over the remaining solution. A Raman microscope system could also allow for the aggregates to be selectively sampled.

5.0   Conclusions

Solutions of PNIPAM microsphere particles were synthesized and studied in DI water, D_2O, and 0.5 M $NaClO_4$ solution using Raman spectroscopy. The PNAIPM particles synthesized in D2O were used to better examine the C-H stretch spectral region as the particles go through the VPT. The downshift in the various C-H vibrational bands shows the dehydration of the isopropyl group of the PNIPAM monomer unit. The highest frequency C-H stretch of the methyl groups

showed the greatest sensitivity to the dehydration and was also complicated the least by other vibrations. The lowest frequency stretch of the C-H group showed a change in frequency at lower temperatures as compared to the other three vibrational bands. This indicates that the dehydration of the amide could be the trigger for dehydration of the monomer unit and the polymer microsphere.

Upon comparison of the PNIPAM particles in DI water to those in 0.5 M $NaClO_4$, a visible aggregation occurs above the LCST for those in the $NaClO_4$ solution. When examining these solutions with UV Resonance Raman spectroscopy, the amide I and amide II vibrational bands give insight into the hydrogen bonding that is occurring. The amide I vibration shows a sharp increase in the relative area of its highest frequency component above the LCST in $NaClO_4$, indicating that more of the amides of the PNIPAM are completely dehydrated. The amide II vibration shows that there are changes in the hydrogen bonding of the amide that differ between the DI water and $NaClO_4$ solution, and possibly indicate an increase in intramolecular hydrogen bonding as the particles aggregate.

6.0 Further Proposed Study to Understand the Volume Phase Transition Mechanism: Utilizing the O-H Stretch Region as a Indication of Hydrophobic Solvation

The O-H stretch region, 3200-3700 cm^{-1}, of the PNIPAM Raman spectra can also be utilized to further the understanding of the mechanism of the VPT of PNIPAM. Through the monitoring of this spectral region, we will be able to further understand the water that is directly hydrogen bonding to an amide group of PNIPAM as well as the waters directly interacting with the

hydrophobic isopropanol groups. The presence of "dangling" O-H groups in a solution can be identified in the Raman spectra with the presence of a vibrational band around 2660cm^{-1} [76-79]. As the PNIPAM particle collapses, the number of proximal waters should decrease and the number of tetrahedral structured bulk water should increase leading to a decrease in the area of the ~3660cm^{-1} band[58]. Although some work in this area has already been done by Terada et al[55], there was no attempt to quantify the changes in the O-H stretch region of PNIPAM solution spectra over the VPT.

For any of the water studies to be completed, it would be optimal to have a close-packed system of PNIPAM particles similar to those that have already been prepared by the Asher group[26]. By using close-packed particles, we can more closely examine the proximal waters without the overwhelming contribution of bulk water.

References

(1)   Pimenov, K. V. 2007.

(2)   Heskins, M.; Guillet, J. E. *Journal of Macromolecular Science: Part A e   Chemistry* **1968**, *2*, 1441.

(3)   Tanaka, T.; Nishio, I.; Sun, S.P   T.; UenoP   Nishio, S. *Science* **1982**, *218*, 467.

(4)   Li, Y.; Tanaka, T. *Annu. Re.v Mater. Sci.* **1992**, *22*, 243.

(5)   Tanaka, T. In *Polyelectrolyte Gels*; American Chemical Society: 1992; Vol. 480, p 1.

(6)   Schild, H. G.; Muthukumar, M.; Tirrell, D. A. *Macromolecules* **1991**, *24*, 948. (7) Marchetti, M.; Prager, S.; Cussler, E. L. *Macromolecules* **1990**, *23*, 1760.

(8)   Hoffman, A. S.; Chen, G. H.; Kaang, S. Y.; Ding, Z. L.; Randeri, K.; Kabra, B. In *Advanced Biomaterials in Biomedical Engineering and Drug Delivery Systems*; Ogata, N., Kim, S., Feijen, J., Okano, T., Eds.; Springer Japan: 1996, p 62.

(9)   Schmaljohann, D. *Advanced Drug Delivery Reviews* **2006**, *58*, 1655.

(10)   Constantin, M.; Cristea, M.; Ascenzi, P.; Fundueanu, G. *Express Polymer Letters* **2011**, *5*, 839.

(11)   BarP   Cohen, Y. In *Proceedings of the 42nd AIAA Structures, Structural Dynamics and Materials Conference (SDM)*; American Institute of Aerospace and Astronautics, Inc. : Seattle, WA, 2001.

(12)   Oktar, O.; Caglar, P.; Seitz, W. R. *Sensors and Actuators B: Chemical* **2005**, *104*, 179.

(13)   Asher, S. A.; Sharma, A. C.; Goponenko, A. V.; Ward, M. M. *Analytical Chemistry* **2003**, *75*, 1676.

(14)   Asher, S. A.; Alexeev, V. L.; Goponenko, A. V.; Sharma, A. C.; Lednev, I. K.; Wilcox, C. S.; Finegold, D. N. *Journal of the American Chemical Society* **2003**, *125*, 3322. (15) Holtz, J. H.; Asher, S. A. *Nature* **1997**, *389*, 829.

(16)   Alexeev, V. L.; Das, S.; Finegold, D. N.; Asher, S. A. *Clinical Chemistry* **2004**, *50*, 2353.

(17)   Richter, A.; Howitz, S.; Kuckling, D.; Arndt, K.P   F. *Sensors and Actuators B: Chemical* **2004**, *99*, 451.

(18)   Harmon, M. E.; Tang, M.; Frank, C. W. *Polymer* **2003**, *44*, 4547.

(19)   Yu, C.; Mutlu, S.; Selvaganapathy, P.; Mastrangelo, C. H.; Svec, F.; Fréchet, J. M. J. *Analytical Chemistry* **2003**, *75*, 1958.

(20)   Debord, J. D.; Lyon, L. A. *The Journal of Physical Chemistry B* **2000**, *104*, 6327.

(21)   Li, S. K.; D'Emanuele, A. *International Journal of Pharmaceutics* **2003**, *267*, 27. (22) Okada, Y.; Tanaka, F. *Macromolecules* **2005**, *38*, 4465.

(23)   Hirokawa, Y.; Tanaka, T. *The Journal of Chemical Physics* **1984**, *81*, 6379.

(24)   Flory, P. J. *The Journal of Chemical Physics* **1942**, *10*, 51.

(25)   Weissman, J. M.; Sunkara, H. B.; Tse, A. S.; Asher, S. A. *Science* **1996**, *274*, 959. (26) Reese, C. E.; Mikhonin, A. V.; Kamenjicki, M.; Tikhonov, A.; Asher, S. A. *Journal of the American Chemical Society* **2004**, *126*, 1493.

(27)   Ahmed, Z.; Gooding, E. A.; Pimenov, K. V.; Wang, L.; Asher, S. A. *The Journal of Physical Chemistry B* **2009**, *113*, 4248.

(28)   Wang, J.; Gan, D.; Lyon, L. A.; ElP   Sayed, M. A. *Journal of the American Chemical Society* **2001**, *123*, 11284.

(29)   Okajima, T.; Harada, I.; Nishio, K.; Hirotsu, S. *The Journal of Chemical Physics* **2002**, *116*, 9068.

(30)   Matsuo, E. S.; Tanaka, T. *The Journal of Chemical Physics* **1988**, *89*, 1695.

(31)   Li, Y.; Tanaka, T. *The Journal of Chemical Physics* **1990**, *92*, 1365.

(32)   Katsumoto, Y.; Tanaka, T.; Sato, H.; Ozaki, Y. *The Journal of Physical Chemistry A* **2001**, *106*, 3429.

(33)   Okada, Y.; Tanaka, F.; Kujawa, P.; Winnik, F. M. *The Journal of Chemical Physics* **2006**, *125*, 244902.

(34)   Otake, K.; Inomata, H.; Konno, M.; Saito, S. *Macromolecules* **1990**, *23*, 283.

(35)   Ghugare, S. V.; Chiessi, E.; Telling, M. T. F.; Deriu, A.; Gerelli, Y.; Wuttke, J.; Paradossi, G. *The Journal of Physical Chemistry B* **2010**, *114*, 10285.

(36)   Sun, S.; Hu, J.; Tang, H.; Wu, P. *The Journal of Physical Chemistry B* **2012**, *114*, 9761.

(37)   Lai, H.; Wu, P. *Polymer* **2010**, *51*, 1404.

(38)   Ono, Y.; Shikata, T. *The Journal of Physical Chemistry B* **2007**, *111*, 1511.

(39)   Ono, Y.; Shikata, T. *Journal of the American Chemical Society* **2006**, *128*, 10030.

(40)   Kumar, S.; Tsai, C.-J.; Nussinov, R. *Biochemistry* **2002**, *41*, 5359.

(41)   Kumar, S.; Tsai, C. J.; Nussinov, R. *Biochemistry* **2003**, *42*, 4864.

(42)   Tanford, C. *Hydrophobic Effect: Formation of Micelles and Biological Membranes*; Wiley: New York, 1973.

(43)   Wang, X.; Wu, C. *Macromolecules* **1999**, *32*, 4299.

(44)   Howe, A. M.; Desrousseaux, S.; Lunel, L. S.; Tavacoli, J.; Yow, H. N.; Routh, A. F. *Advances in Colloid and Interface Science* **2009**, *147–148*, 124.

(45)   Kubota, K.; Fujishige, S.; Ando, I. *The Journal of Physical Chemistry* **1990**, *94*, 5154.

(46)   Schild, H. G.; Tirrell, D. A. *The Journal of Physical Chemistry* **1990**, *94*, 4352.

(47)   Maeda, Y.; Higuchi, T.; Ikeda, I. *Langmuir* **2000**, *16*, 7503.

(48)   Maeda, Y.; Nakamura, T.; Ikeda, I. *Macromolecules* **2001**, *34*, 8246.

(49)   Ramon, O.; Kesselman, E.; Berkovici, R.; Cohen, Y.; Paz, Y. *Journal of Polymer Science Part B: Polymer Physics* **2001**, *39*, 1665.

(50)   Chen, X. G.; SchweitzerP   Stenner, R.; Asher, S. A.; Mirkin, N. G.; Krimm, S. *The Journal of Physical Chemistry* **1995**, *99*, 3074.

(51)   Myshakina, N. S.; Ahmed, Z.; Asher, S. A. *The Journal of Physical Chemistry B* **2008**, *112*, 11873.

(52)   Annaka, M.; Amo, Y.; Sasaki, S.; Tominaga, Y.; Motokawa, K.; Nakahira, T. *Physical Review E* **2002**, *65*, 031805.

(53)   Annaka, M.; Motokawa, K.; Sasaki, S.; Nakahira, T.; Kawasaki, H.; Maeda, H.; Amo, Y.; Tominaga, Y. *The Journal of Chemical Physics* **2000**, *113*, 5980.

(54)   Suzuki, Y.; Suzuki, N.; Takasu, Y.; Nishio, I. *The Journal of Chemical Physics* **1997**, *107*, 5890.

(55)   Terada, T.; Inaba, T.; Kitano, H.; Maeda, Y.; Tsukida, N. *Macromolecular Chemistry and Physics* **1994**, *195*, 3261.

(56) Deshmukh, S.; Mooney, D. A.; McDermott, T.; Kulkarni, S.; Don MacElroy, J. M. *Soft Matter* **2009**, *5*, 1514.

(57) Deshmukh, S. A.; Sankaranarayanan, S. K. R. S.; Suthar, K.; Mancini, D. C. *The Journal of Physical Chemistry B* **2012**, *116*, 2651.

(58) Deshmukh, S. A.; Sankaranarayanan, S. K. R. S.; Mancini, D. C. *The Journal of Physical Chemistry B* **2012**, *116*, 5501.

(59) Asher, S. A. *Analytical Chemistry* **1993**, *65*, 201A.

(60) Asher, S. A. *Analytical Chemistry* **1993**, *65*, 59A.

(61) Chi, Z.; Chen, X. G.; Holtz, J. S. W.; Asher, S. A. *Biochemistry* **1998**, *37*, 2854. (62) Mikhonin, A. V.; Bykov, S. V.; Myshakina, N. S.; Asher, S. A. *The Journal of Physical Chemistry B* **2006**, *110*, 1928.

(63) Lednev, I. K.; Karnoup, A. S.; Sparrow, M. C.; Asher, S. A. *Journal of the American Chemical Society* **1999**, *121*, 8074.

(64) Schmidt, P.; Dybal, J.; Trchová, M. *Vibrational Spectroscopy* **2006**, *42*, 278.

(65) Hobza, P.; Havlas, Z. k. *Chemical Reviews* **2000**, *100*, 4253.

(66) Gu, Y.; Kar, T.; Scheiner, S. *Journal of the American Chemical Society* **1999**, *121*, 9411.

(67) Hermansson, K. *The Journal of Physical Chemistry A* **2002**, *106*, 4695.

(68) Masunov, A. m.; Dannenberg, J. J.; Contreras, R. n. H. *The Journal of Physical Chemistry A* **2001**, *105*, 4737.

(69) Qian, W.; Krimm, S. *The Journal of Physical Chemistry A* **2002**, *106*, 6628.

(70) Green, J. H. S. *Transactions of the Faraday Society* **1963**, *59*, 1559.

(71) Evans, J. C.; Bernstein, H. J. *Canadian Journal of Chemistry* **1956**, *34*, 1037.

(72) Routh, A. F.; Vincent, B. *Langmuir* **2002**, *18*, 5366.

(73) Daly, E.; Saunders, B. R. *Langmuir* **2000**, *16*, 5546.

(74) Hall, R. J.; Pinkrah, V. T.; Chowdhry, B. Z.; Snowden, M. J. *Colloids and Surfaces A: Physicochemical and Engineering Aspects* **2004**, *233*, 25.

(75) Bykov, S.; Lednev, I.; Ianoul, A.; Mikhonin, A.; Munro, C.; Asher, S. A. *Applied Spectroscopy* **2005**, *59*, 3074.

(76) Tomlinson-Phillips, J.; Davis, J.; Ben-Amotz, D.; Spångberg, D.; Pejov, L.; Hermansson, K. *The Journal of Physical Chemistry A* **2011**, *115*, 6177.

(77) Scatena, L. F.; Richmond, G. L. *The Journal of Physical Chemistry B* **2001**, *105*, 11240.

(78) Scatena, L. F.; Brown, M. G.; Richmond, G. L. *Science* **2001**, *292*, 908.

(79) Perera, P. N.; Fega, K. R.; Lawrence, C.; Sundstrom, E. J.; Tomlinson-Phillips, J.; Ben-Amotz, D. *Proceedings of the National Academy of Sciences* **2009**, *106*, 12230.